Multiparticle Correlations in Mesoscopic Scattering: Boson Sampling, Birthday Paradox, and Hong-Ou-Mandel Profiles

Juan-Diego Urbina,[1] Jack Kuipers,[1] Sho Matsumoto,[2] Quirin Hummel,[1] and Klaus Richter[1]
[1]*Institut für Theoretische Physik, Universität Regensburg, D-93040 Regensburg, Germany*
[2]*Graduate School of Science and Engineering, Kagoshima University, 1-21-35 Korimoto, Kagoshima, Japan*
(Received 18 August 2014; revised manuscript received 15 September 2015; published 8 March 2016)

The interplay between single-particle interference and quantum indistinguishability leads to signature correlations in many-body scattering. We uncover these with a semiclassical calculation of the transmission probabilities through mesoscopic cavities for systems of noninteracting particles. For chaotic cavities we provide the universal form of the first two moments of the transmission probabilities over ensembles of random unitary matrices, including weak localization and dephasing effects. If the incoming many-body state consists of two macroscopically occupied wave packets, their time delay drives a quantum-classical transition along a boundary determined by the bosonic birthday paradox. Mesoscopic chaotic scattering of Bose-Einstein condensates is, then, a realistic candidate to build a boson sampler and to observe the macroscopic Hong-Ou-Mandel effect.

DOI: 10.1103/PhysRevLett.116.100401

In quantum mechanics, identical particles are indistinguishable and their very identity is, then, affected by quantum fluctuations and interference effects. A prominent type of many-body (MB) correlations is exemplified by the celebrated Hong-Ou-Mandel (HOM) effect [1], by now the standard indicator of MB coherence in quantum optics. There, the probability of observing two photons leaving in different arms of a beam splitter is measured. As a function of the delay between the arrival times of the incoming pulses, the coincidence probability shows a characteristic dip that can be seen as an effective quantum-classical transition (QCT), where the difference in arrival times dephases the MB interference due to quantum indistinguishability [2]. In recent years, a wealth of hallmark experimental studies of MB scattering has gone beyond this scenario [3–9]. The aim is to reach a regime where for a random single-particle (SP) scattering matrix σ, and due to MB interference, the complexity in the calculation of MB scattering probabilities as a function of σ beats classical computers; this is called the boson sampling (BS) problem [10]. However, while current optical devices [5,9] reach photon occupations (below 6) far from the required regime of large number of particles, it is not clear how to sample σ uniformly on platforms based on trapped ions [11], cold atoms [12], and spin chains [13].

Here we study mesoscopic MB scattering of massive particles depicted in Fig. 1(a). While formally identical to the optical situation in that it relates SP scattering matrices with MB scattering probabilities, it allows for large occupations through, e.g., Bose-Einstein condensation. Moreover, a standard result from quantum chaos [14] says that complex SP interference due to classical chaos inside such a mesoscopic scattering cavity Ω transforms averages over small changes of the incoming energies into averages over an appropriate ensemble of unitary matrices, thus providing a genuine sampling over random scattering matrices. With experimental techniques for preparation

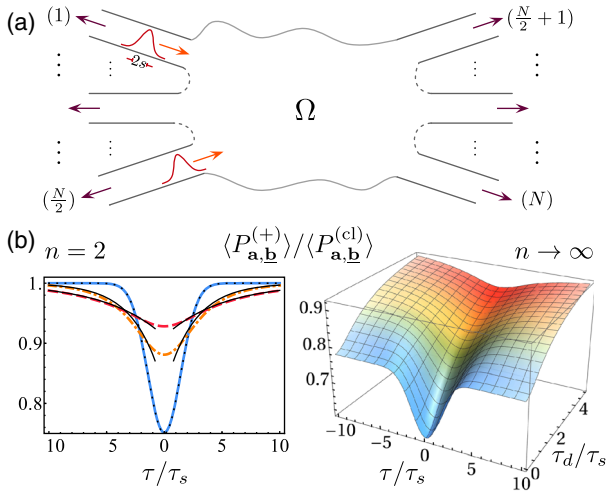

FIG. 1. (a) Two bosonic wave packets with mean velocity v, transversal channels $\mathbf{a}=(a_1,a_2)$, and width $s=v\tau_s$ approach the chaotic cavity Ω with mean position difference $z=v\tau$. (b) Ratio $\langle P^{(+)}\rangle/\langle P^{(\mathrm{cl})}\rangle$, between the quantum and classical probabilities (averaged over mesoscopic fluctuations), to find the bosonic particles in different output channels $\underline{\mathbf{b}}$. Left: For singly occupied wave packets, $n=2$ (with $N=4$ channels), we observe a generalized HOM profile that changes from Gaussian (dotted) to a universal exponential (thin solid tails) as function of the cavity's dwell time τ_d, with $\tau_d/\tau_s=0.1, 2.5, 5$ (solid blue, dashed-dotted yellow, dashed red) [Eqs. (10)–(12) with $z=z_{12}$]. Right: For $n\to\infty$, $N=\alpha n^{\eta}$, $\langle P^{(+)}\rangle$ reaches its classical limit if $\eta>2$ or trivially saturates due to the bosonic birthday paradox (BBP) for $\eta<2$. For $\eta=2$, the quantum-classical transition shows an exponentiated HOM-like profile [Eq. (16) with $x=0$, $\alpha=1$].

of coherent macroscopic occupations [15], chaotic scattering [16], and detection [17], mesoscopic scattering of Bose-Einstein condensates contains all prerequisites of a realistic platform for BS, its certification [18], and related tasks [19]. This is illustrated with the recent realization of the two-particle HOM effect using atomic beam splitters in [22].

Because the methods developed for the study of MB scattering of photons [23–27] ignore mesoscopic effects and physical scales like the cavity's dwell time, we fill this gap and present analytic results on coherent MB scattering in the mesoscopic regime, particularly the way the QCT is affected by large occupation numbers and mesoscopic fluctuations. Supported by the universal correlations of SP scattering matrices [28,29] responsible for characteristic mesoscopic wave interference effects like weak localization [30] and universal conductance fluctuations [31], we address the emergence of universal MB correlations due to the interplay between classical ergodicity, SP interference, and quantum indistinguishability well beyond the standard semiclassical SP picture (see, for instance, [32]). Despite their intrinsically nonclassical character, here MB correlations are successfully expressed and computed within a semiclassical approach in terms of interfering SP classical paths in the spirit of the Feynman path integral [33] by a one-to-one correspondence between MB classical paths (illustrated in Fig. 2) and terms of the expansion of the MB scattering probabilities. Our complete enumeration and classification of the MB paths allows for an explicit analysis of emergent phenomena in the thermodynamic many-particle limit, something out of reach of leading-order random matrix theory (RMT) methods [34–36].

We also show here how mesoscopic dephasing effects encoded in the dwell time lead eventually to a universal HOM profile, and provide a mesoscopic approach to the BBP that constrains the experimental realization of BS due to a counterintuitive scaling of coincidence probabilities with the density of particles [37]. Our methods can be extended to the optical case by using the dispersion relation for photons and changing the cavity Ω to a multiport waveguide network, making a connection with recent experiments [6–9].

The setup of the mesoscopic many-body scattering problem is depicted in Fig. 1(a). The incoming particles $(i = 1, \ldots, n)$ with positions (x_i, y_i) occupy SP states represented by normalized wave packets

$$\phi_i(x_i, y_i) \propto e^{-ikx_i} X(x_i - z_i)\chi_{a_i}(y_i). \tag{1}$$

The longitudinal wave packets $e^{-ikx}X(x - z)$ have variance s^2, mean initial position $z \gg s$, and approach the cavity Ω with mean momentum $\hbar k = mv > 0$ along the longitudinal directions $-x_i$. The relative positions of the incoming particles are then parametrized by the differences $z_{ij} = z_i - z_j$ or delay times $\tau_{ij} = z_{ij}/v$. The transverse wave function in the incoming channel $a_i \in \{1, \ldots, N/2\}$ is $\chi_{a_i}(y_i)$ and has energy E_χ, assumed for simplicity to be identical for all channels.

If the particles are identical, quantum indistinguishability demands their joint state to be symmetrized according to their spin [38]. Introducing $\epsilon = -1(+1)$ for fermions (bosons), the symmetrized amplitude to find the particles leaving in channels $\mathbf{b} = (b_1, \ldots, b_n)$ with energies $\mathbf{E} = (E_1, \ldots, E_n)$ is given by a sum over the action of the $n!$ elements $\mathcal{P}$ of the permutation group,

$$A^{(\epsilon)}_{\mathbf{a},\mathbf{b}}(\mathbf{E}) = \sum_{\mathcal{P}} \epsilon^{\mathcal{P}} A_{\mathbf{a},\mathcal{P}\mathbf{b}}(\mathcal{P}\mathbf{E}), \tag{2}$$

on the scattering amplitude for distinguishable particles,

$$A_{\mathbf{a},\mathbf{b}}(\mathbf{E}) = \prod_{i=1}^{n} \sqrt{\frac{m}{\hbar}} \frac{e^{-i(k-q_i)z_i}}{\sqrt{2\pi\hbar q_i}} \tilde{X}(k - q_i)\sigma_{b_i,a_i}(E_i), \tag{3}$$

where $\hbar q_i = \sqrt{2m(E_i - E_\chi)}$ and $\tilde{X}(k) = \int e^{-ikx}X(x)dx$. When $n = 1$, Eq. (3) formally defines the SP scattering matrix $\sigma_{b,a}(E)$ connecting the incoming and outgoing channels a and b. With these definitions, the MB probability to find the particles leaving in channels $\mathbf{b}$ but regardless of their energies is given by

$$\begin{aligned} P^{(\epsilon)}_{\mathbf{a},\mathbf{b}} &= \frac{1}{\mathbf{a}!\mathbf{b}!} \int_{E_\chi}^{\infty} d\mathbf{E} |A^{(\epsilon)}_{\mathbf{a},\mathbf{b}}(\mathbf{E})|^2 \\ &= \frac{1}{\mathbf{a}!\mathbf{b}!} \sum_{\mathcal{P},\mathcal{P}'} \epsilon^{\mathcal{P}+\mathcal{P}'} \int_{E_\chi}^{\infty} d\mathbf{E} A_{\mathbf{a},\mathcal{P}\mathbf{b}}(\mathcal{P}\mathbf{E}) A^*_{\mathbf{a},\mathcal{P}'\mathbf{b}}(\mathcal{P}'\mathbf{E}). \end{aligned} \tag{4}$$

Equation (4) includes the normalization factors $\mathbf{o}! = \prod_i \mathrm{mul}(o_i)!$, where $\mathrm{mul}(o_i)$ is the multiplicity of the channel index o_i, in order to have $\sum_{b_1 \le \cdots \le b_n}^{n} P^{(\epsilon)}_{\mathbf{a},\mathbf{b}} = 1$.

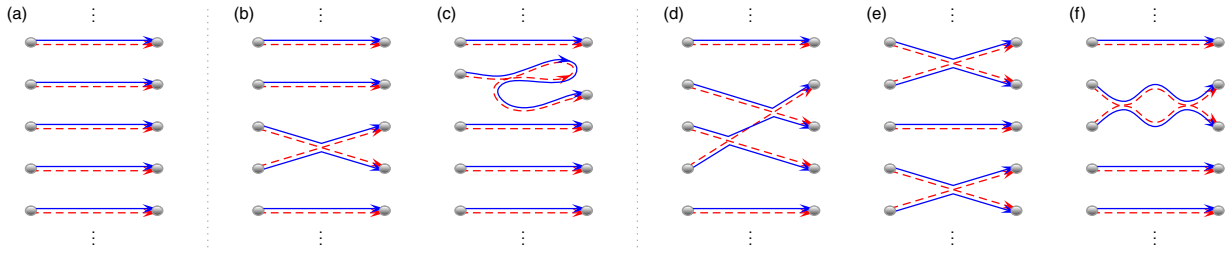

FIG. 2. Sets of interfering SP paths required for calculating MB transition probabilities, here for $n = 5$. In (a), both SP and MB correlations are neglected. In (c), weak localization at the SP level is included. For (b), (d), (e), and (f) only MB correlations are included. Combined SP and MB effects appear when the links in a MB diagram are decorated with SP loops.

Because of interference between different ($\mathcal{P} \neq \mathcal{P}'$) distinguishable MB configurations, $P^{(\epsilon)}_{\mathbf{a},\mathbf{b}}$ is sensitive to the relative positions of the incoming wave packets z_{ij}. This dependence drives a transition from indistinguishability to effective distinguishability for $z_{ij} \to \infty$. MB interference due to indistinguishability is thus intrinsically dephased, and one observes an effective QCT [8,9], as seen from the HOM scenario [1] where σ is $\mathbf{E}$ independent and $2n = 4 = N$. In this case we get, using Eq. (4),

$$P^{\mathrm{HOM}}_{a_1\neq a_2, b_1\neq b_2} = \frac{|[\sigma]|^2+1}{2} + \epsilon\frac{|[\sigma]|^2-1}{2}\mathcal{F}^2(z_{12}), \quad (5)$$

where $[\cdots]$ denotes permanent (unsigned determinant) and

$$\mathcal{F}(z) = \int_{-\infty}^{\infty} X(x)X(x-z)dx, \quad (6)$$

satisfying $\mathcal{F}(0) = 1$, $\mathcal{F}(\infty) = 0$, is responsible for the nonuniversal profile of the QCT, as shown in the dotted curve in the left panel of Fig. 1(b) for Gaussian wave packets.

Individual σ matrices with specific entries leading to Eq. (5) and its few-particle generalizations are routinely constructed in arrays of beam splitters connecting waveguides for photonic systems [6,7,24,25] and in quantum point contacts for electrons occupying edge states [39,40]. Thanks to the Bohigas-Gianonni-Schmidt conjecture, replacing the beam splitter or point contact by a chaotic mesoscopic cavity allows us to sample the moments $\langle f(\sigma)^\mu\rangle$ of any observable $f(\sigma)$ over the full ensemble of random, unitary matrices σ by sampling over energy windows or small variations of the cavity [14]. In this case, averages of the form $\langle \sigma_{b,a}(E)\sigma^*_{b',a'}(E')\rangle$ display universal features depending only on the presence or absence of time-reversal invariance, denoted as the orthogonal ($\beta = 1$) and unitary ($\beta = 2$) case. Interference effects in SP scattering probabilities are semiclassically understood in terms of statistical correlations among classical actions [28–31,41] and here we generalize these methods.

We will mainly focus on the case, denoted by $\underline{\mathbf{b}}$, where every output channel is singly occupied; for $\beta = 1$ we also demand that the in- and outgoing channels are different. In our approach, any $2n\mu$-order correlator of σ matrices appearing in the moments $\langle|P^{(\epsilon)}_{\mathbf{a},\underline{\mathbf{b}}}(\mathbf{E})|^{2\mu}\rangle$ of the distribution of scattering probabilities, Eq. (4), is given by an infinite diagrammatic expansion with terms that can be visualized as a set of links joining $n\mu$ in and outgoing channels, see Fig. 2. For the averaged transition probability, $\mu = 1$, the classical limit

$$\langle P^{(\mathrm{cl})}_{\mathbf{a},\mathbf{b}}\rangle = (n!/\mathbf{b}!)N^{-n}, \quad (7)$$

for general $\mathbf{b}$, is obtained from the trivial topology in Fig. 2(a) [42]. In Eq. (7), N is the number of open channels at the mean initial SP energy $U = mv^2/2 + E_\chi$. Quantum effects at the SP level, in the spirit of [29,30], give the sole contribution for $\mathcal{P} = \mathcal{P}'$ in Eq. (4) and are generated by adding SP loops to the links, as in Fig. 2(c). These terms, independent of ϵ, can be evaluated up to infinite order to give (with $\langle P^{(\mathrm{cl})}_{\mathbf{a},\underline{\mathbf{b}}}\rangle = n!N^{-n}$)

$$\langle P^{(\mathrm{SP})}_{\mathbf{a},\underline{\mathbf{b}}}\rangle = \langle P^{(\mathrm{cl})}_{\mathbf{a},\underline{\mathbf{b}}}\rangle[1-(1-2/\beta)/N]^{-n}. \quad (8)$$

To calculate $\langle P^{(\epsilon)}_{\mathbf{a},\underline{\mathbf{b}}}\rangle$ we must include genuine MB effects characterized by correlations between different SP paths, $\mathcal{P} \neq \mathcal{P}'$. The first MB diagrams without SP loops are depicted in Figs. 2(b),2(d), and 2(e), while Fig. 2(f) shows the diagram in Fig. 2(b) with a loop between two particles. The basic correlator in Fig. 2(b) involving a single pair of correlated paths is [31,43]

$$\langle \sigma_{b_i,a_i}(E_i)\sigma_{b_j,a_j}(E_j)\sigma^*_{b_i,a_j}(E_j)\sigma^*_{b_j,a_i}(E_i)\rangle = \frac{1}{N^3}\frac{\hbar^2}{\hbar^2+\tau_d^2(E_i-E_j)^2} + \mathcal{O}\left(\frac{1}{N^4}\right), \quad (9)$$

where τ_d is the dwell time, the average time a particle with energy $(E_i + E_j)/2$ remains within Ω. Taking into account only pairs of correlated paths, Eq. (4) gives [44]

$$\frac{\langle P^{(\epsilon)}_{\mathbf{a},\underline{\mathbf{b}}}\rangle}{\langle P^{\mathrm{cl}}_{\mathbf{a},\underline{\mathbf{b}}}\rangle} = \frac{\langle P^{(\mathrm{SP})}_{\mathbf{a},\underline{\mathbf{b}}}\rangle}{\langle P^{\mathrm{cl}}_{\mathbf{a},\underline{\mathbf{b}}}\rangle} - \frac{\epsilon}{N}\sum_{i<j}^{n}\mathcal{Q}^{(2)}(z_{ij}) + \mathcal{O}\left(\frac{1}{N^2}\right), \quad (10)$$

with the generalized overlap integral Eq. (6),

$$\mathcal{Q}^{(2)}(z) = \int_{-\infty}^{\infty}\mathcal{F}^2(z-vt)\frac{e^{-|t|/\tau_d}}{2\tau_d}dt. \quad (11)$$

In order to study the impact of mesoscopic effects in the HOM scenario we take $n = 2$, and the sum in our Eq. (10) reduces to a single contribution with $i = 1$, $j = 2$. In the left panel of Fig. 1(b) we plot $\langle P^{(\epsilon)}_{\mathbf{a},\underline{\mathbf{b}}}\rangle/\langle P^{\mathrm{cl}}_{\mathbf{a},\underline{\mathbf{b}}}\rangle$ as function of the mismatch distance $z = z_{12}$ between the incoming wave packets in the case of broken time-reversal invariance where Eq. (8) gives $\langle P^{(\mathrm{SP})}_{\mathbf{a},\underline{\mathbf{b}}}\rangle = \langle P^{(\mathrm{cl})}_{\mathbf{a},\underline{\mathbf{b}}}\rangle$. We see how mesoscopic effects produce universal deviations from the usual Gaussian profile, represented by the dotted line.

The functions $\mathcal{Q}^{(2)}$ determine how the mismatch of arrival times dephases the MB correlations. We interpret Eqs. (10), (11) as follows: Pairs of incoming particles that are effectively distinguishable get to interfere if their time delay τ_{ij} in entering the cavity is compensated by the time τ_d the first particle is held within the mesoscopic scattering region. However, the interference gets weighted by the survival probability $e^{-t/\tau_d}/\tau_d$ of remaining inside the chaotic scatterer Ω. Universality of the dephasing of MB correlations is expected if τ_d competes with the delay times τ_{ij} and widths $\tau_s = s/v$ of the incoming wave packets, and leads to exponential tails in the interference profile for $|z_{ij}| \gg s$. As shown in the left panel of Fig. 1(b), these exponential regions grow with the ratio τ_d/τ_s; for $\tau_d \leq \tau_s$,

on the other hand, QCT depends on the shape of the incoming wave packets, as in Eq. (5),

$$\mathcal{Q}^{(2)}(z)\begin{cases} \xrightarrow{v\tau_d \gg v\tau_s > k^{-1}} & \left(\int_{-\infty}^{\infty}\mathcal{F}^2(z)\frac{dz}{s}\right)\frac{e^{-|z|/v\tau_d}}{2\tau_d/\tau_s} \\ \xrightarrow{v\tau_s \gg v\tau_d > k^{-1}} & \mathcal{F}^2(z). \end{cases} \tag{12}$$

Mesoscopic dephasing of two-particle interference plays a fundamental role in the thermodynamic limit $N, n \to \infty$ of the QCT through the mesoscopic version of the BBP [37], which constrains the scaling $N = \alpha n^\eta$ in such a way that $\langle P^{(\epsilon)}_{\mathbf{a},\mathbf{b}}\rangle$ does not get trivially saturated either classically or by quantum bunching and antibunching [3,10,37,45,46]. To achieve a semiclassical theory of the mesoscopic BBP, in [47] we use RMT techniques to calculate $\langle P^{(\epsilon)}_{\mathbf{a},\mathbf{b}}\rangle$, which is only possible for $z_{ij} = 0$, $\tau_d/\tau_s = 0$. We obtain the expression, valid for arbitrary ϵ, N, n, $\mathbf{a}$, $\mathbf{b}$ if $\beta = 2$ and with the only condition $\mathbf{a}\cap\mathbf{b} = \emptyset$ if $\beta = 1$,

$$\langle P^{(\epsilon)}_{\mathbf{a},\mathbf{b}}\rangle|^{\tau_d/\tau_s=0}_{z_{ij}=0} = \frac{\mathcal{W}^{(\epsilon)}_\beta(N,n)n!}{\prod_{l=0}^{n-1}(N+\epsilon l)}(\delta_{\epsilon,+} + \delta_{\epsilon,-}\delta_{\mathbf{b},\underline{\mathbf{b}}}), \tag{13}$$

with $\delta_{\mathbf{b},\underline{\mathbf{b}}} = 1(0)$ if $\mathbf{b}$ is (is not) singly occupied and

$$\mathcal{W}^{(\epsilon)}_1(N,n) = \frac{N+\epsilon(n-1)}{N+n+\epsilon(n-1)}, \qquad \mathcal{W}^{(\epsilon)}_2(N,n) = 1. \tag{14}$$

Equation (13) is a generalization for arbitrary β and ϵ of the bosonic, unitary case reported in [37]. A key observation is that, contrary to the distinguishable (classical) case [Eq. (7)], result (13) is constant over the MB final states for $\beta = 2$. SP chaos leads then to full MB equilibration for systems with broken time-reversal symmetry, providing dynamical support to the analysis of [37].

For singly occupied states $\underline{\mathbf{b}}$, Eqs. (7), (13) give

$$\left(\frac{\langle P^{(\epsilon)}_{\mathbf{a},\underline{\mathbf{b}}}\rangle}{\langle P^{(\mathrm{cl})}_{\mathbf{a},\underline{\mathbf{b}}}\rangle}\right)^{\epsilon}\Bigg|^{\tau_d/\tau_s=0}_{z_{ij}=0} \xrightarrow[N=\alpha n^\eta]{n\gg 1} \begin{cases} 0 & \text{for } \eta < 2 \\ e^{-1/2\alpha} & \text{for } \eta = 2 \\ 1 & \text{for } \eta > 2, \end{cases} \tag{15}$$

showing how, in the thermodynamic limit, scattering of identical particles is classical in the dilute limit $\eta > 2$, it gets saturated due to boson bunching and fermion antibunching even at zero densities if $\eta < 2$, and only the scaling $N = \alpha n^2$ gives a nontrivial limit. This is the essence of the BBP [10,37,45,46], here derived from RMT arguments (and for $\eta > 1$ from semiclassical arguments) for arbitrary β, ϵ. For $\beta = 1$, weak localization corrections to MB equilibration (akin to MB coherent backscattering [48]) to BS and to BBP are obtained from Eq. (13).

To address the interplay between intrinsic ($z_{ij} \neq 0$) and mesoscopic ($\tau_d/\tau_s \neq 0$) dephasing, one must go beyond RMT; we resort to semiclassical diagrammatics. In [49] we study the semiclassical generating function for $\langle P^{(\epsilon)}_{\mathbf{a},\mathbf{b}}\rangle$ and show that, order by order in the $1/N$ expansion, diagrams with pairwise correlations between particles like Figs. 2(b) and 2(e) dominate the $n \to \infty$ limit leading to Eq. (15) for $\eta > 1$. The whole set of semiclasssical diagrams with pairwise correlations can now be constructed for $\tau_d/\tau_s > 0$ and $z_{ij} \neq 0$, and resumed to infinite order where the scaling $\eta = 2$ emerges [50].

If $z_{ij} \in \{0, z\}$, a situation that can be realized for bosons by injecting two wave packets with macroscopic occupations $n(1 \pm x)/2$, we get [51]

$$\frac{\langle P^{(\epsilon)}_{\mathbf{a},\underline{\mathbf{b}}}\rangle}{\langle P^{(\mathrm{cl})}_{\mathbf{a},\underline{\mathbf{b}}}\rangle} \xrightarrow[N=\alpha n^2]{n\gg 1} e^{-(\epsilon/4\alpha)[(1+x^2)\mathcal{Q}^{(2)}(0)+(1-x^2)\mathcal{Q}^{(2)}(z)]}. \tag{16}$$

Remarkably, then, for macroscopically populated incoming states we observe again a QCT driven by the arrival difference, with an exponentiated HOM-like profile, as shown in the right panel of Fig. 1(b) for $x = 0$ and $\alpha = 1$.

Coming back to finite systems where MB interference is affected by other types of correlations, the diagram Fig. 2(d) containing three-body correlations gives

$$\frac{\langle P^{(\epsilon)}_{\mathbf{a},\underline{\mathbf{b}}}\rangle^{\text{triplets}}}{\langle P^{(\mathrm{cl})}_{\mathbf{a},\underline{\mathbf{b}}}\rangle} = \frac{2\epsilon}{N^2}\sum_{i<j<k}\mathcal{Q}^{(3)}(z_{ij}, z_{kj}), \tag{17}$$

with overlapping and exponential regimes given by

$$\mathcal{Q}^{(3)}(z,z')\begin{cases} \xrightarrow{v\tau_d \gg v\tau_s > k^{-1}} & \mathcal{C}^{(3)}\frac{e^{-3\mathrm{Max}(z,z',0)/v\tau_d}}{2\tau_d/\tau_s}\frac{e^{(z+z')/v\tau_d}}{2\tau_d/\tau_s}, \\ \xrightarrow{v\tau_s \gg v\tau_d > k^{-1}} & \mathcal{F}(z)\mathcal{F}(z')\mathcal{F}(z-z') \end{cases} \tag{18}$$

and $\mathcal{C}^{(3)} = s^{-2}\int_{-\infty}^{\infty}\mathcal{F}(z)\mathcal{F}(z')\mathcal{F}(z-z')dzdz'$. As shown in Fig. 3, this transition produces universal dephasing characterized by kinks with threefold symmetry as a function of the time delay between incoming particles, consistent with the correlations measured in [9].

In conclusion, we have presented a semiclassical approach to quantum scattering for many-body systems and used it to study the emergence of universal effects due to the interplay between single-particle classical chaos and quantum correlations coming from indistinguishability. We have explicitly constructed the correlations responsible for

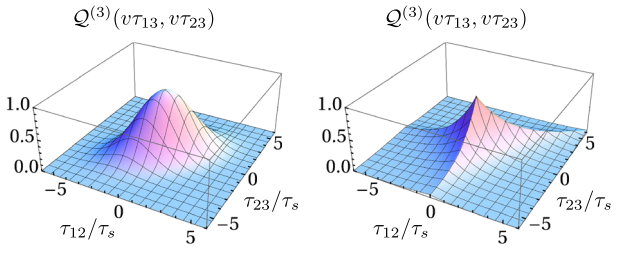

FIG. 3. Transition between the overlapping ($\tau_d/\tau_s = 0.1$, left) and the universal exponential ($\tau_d/\tau_s = 2$, right) regime for the three-body interference term, Eq. (17).

many-body interference in mesoscopic scattering and computed their effect for both small and macroscopically large occupations in the thermodynamic limit, thus opening the possibility of translating boson sampling, the bosonic birthday paradox, and related timely problems into experimentally accessible scenarios of chaotic scattering with massive particles such as cold atoms, as outlined in the beginning of this Letter. Single-particle chaos turns out to be sufficient to achieve many-body ergodicity, and this allows us to compute mesoscopic corrections to the bosonic birthday paradox. It leads to a sharp quantum-classical transition in the thermodynamic limit and, under the scaling for the quantum-classical boundary, we found an exponentiated form of the Hong-Ou-Mandel profile.

Going beyond the first moment $\langle P \rangle$ of the distribution of scattering probabilities, in [52] we further calculate the leading order of the second moment $\langle P^2 \rangle$. In fact, determining just the leading order of higher moments should be pertinent for the permanent anticoncentration conjecture important for boson sampling [10]. Intriguingly, then, semiclassical diagrams and random matrices open up new avenues for understanding permanent statistics, while mesoscopic scattering of massive bosons appears as a promising candidate for their measurement.

We thank Andreas Buchleitner and Malte Tichy for instructive discussions, and an anonymous referee for valuable suggestions and for drawing our attention to Refs. [20,21].

[1] C. K. Hong, Z. Y. Ou, and L. Mandel, Phys. Rev. Lett. **59**, 2044 (1987).
[2] Y.-S. Ra, M. C. Tichy, H.-T. Lim, O. Kwon, F. Mintert, A. Buchleitner, and Y.-H. Kim, Proc. Natl. Acad. Sci. U.S.A. **110**, 1227 (2013).
[3] M. Tillmann, B. Dakic, R. Heilmann, S. Nolte, A. Szameit, and P. Walther, Nat. Photonics **7**, 540 (2013).
[4] M. A. Broome, A. Fedrizzi, S. Rahimi-Keshari, J. Dove, S. Aaronson, T. C. Ralph, and A. G. White, Science **339**, 794 (2013).
[5] A. Crespi, R. Osellame, R. Ramponi, D. J. Brod, E. F. Galvao, N. Spagnolo, C. Vitelli, E. Maiorino, P. Mataloni, and F. Sciarrino, Nat. Photonics **7**, 545 (2013).
[6] J. B. Spring, B. J. Metcalf, P. C. Humphreys, W. S. Kolthammer, X.-M. Jin, M. Barbieri, A. Datta, N. Thomas-Peter, N. K. Langford, D. Kundys, J. C. Gates, B. J. Smith, P. G. R. Smith, and I. A. Walmsley, Science **339**, 798 (2013).
[7] B. J. Metcalf, N. Thomas-Peter, J. B. Spring, D. Kundys, M. A. Broome, P. Humphreys, X.-M. Jin, M. Barbieri, W. S. Kolthammer, J. C. Gates, B. J. Smith, N. K. Langford, P. G. R. Smith, and I. A. Walmsley, Nat. Commun. **4**, 1356 (2013).
[8] Y.-S. Ra, M. C. Tichy, H.-T. Lim, O. Kwon, F. Mintert, A. Buchleitner, and Y.-H. Kim, Nat. Commun. **4**, 2451 (2013).
[9] M. Tillmann, S.-H. Tan, S. E. Stoeckl, B. C. Sanders, H. de Guise, R. Heilmann, S. Nolte, A. Szameit, and P. Walther, Phys. Rev. X **5**, 041015 (2015).
[10] S. Aaronson and A. Arkhipov, in *Proceedings of the 43rd Annual ACM Symposium on Theory of Computing (STOC '11)* (ACM, New York, 2011), pp. 333–342.
[11] C. Shen, Z. Zhang, and L. M. Duan, Phys. Rev. Lett. **112**, 050504 (2014).
[12] T. Engl, J. D. Urbina, Q. Hummel, and K. Richter, Ann. Phys. (Berlin) **527**, 737 (2015).
[13] B. Peropadre, A. Aspuru-Guzik, and J. J. Garcia-Ripoll, arXiv:1509.02703.
[14] F. Haake, *Quantum Signatures of Chaos* (Springer, Berlin, 2010).
[15] M. R. Andrews, C. G. Townsend, H.-J. Miesner, D. S. Durfee, D. M. Kurn, and W. Ketterle, Science **275**, 637 (1997).
[16] G. L. Gattobigio, A. Couvert, B. Georgeot, and D. Guery-Odelin, Phys. Rev. Lett. **107**, 254104 (2011).
[17] J. F. Sherson, C. Weitenberg, M. Endres, M. Cheneau, I. Bloch, and S. Kuhr, Nature (London) **467**, 68 (2010).
[18] M. Walschaers, J. Kuipers, J. D. Urbina, K. Mayer, M. C. Tichy, K. Richter, and A. Buchleitner, arXiv:1410.8547 [New J. Phys. (to be published)].
[19] Because of the formal analogy with photonic systems, in the limit of structureless cavities ($\tau_d \to 0$), our mesoscopic BS can be also used to implement tasks like simulating vibronic spectra in molecules [20] and generating massive path entanglement for metrology applications as in [21].
[20] J. Huh, G. G. Guerreschi, B. Peropadre, J. R. McClean, and A. Aspuru-Guzik, Nat. Photonics **9**, 615 (2015).
[21] K. R. Motes, J. P. Olson, E. J. Rabeaux, J. P. Dowling, S. J. Olson, and P. P. Rohde, Phys. Rev. Lett. **114**, 170802 (2015).
[22] R. Lopes, A. Imanaliev, A. Aspect, M. Cheneau, D. Boiron, and C. I. Westbrook, Nature (London) **520**, 66 (2015).
[23] M. C. Tichy, M. Tiersch, F. de Melo, F. Mintert, and A. Buchleitner, Phys. Rev. Lett. **104**, 220405 (2010).
[24] S. Aaronson and A. Arkhipov, Quant. Inf. Comp. **14**, 1383 (2014).
[25] P. P. Rhode, K. R. Motes, P. A. Knott, J. Fitzsimons, W. J. Munro, and J. P. Dowling, Phys. Rev. A **91**, 012342 (2015).
[26] C. Gogolin, M. Kliesch, L. Aolita, and J. Eisert, arXiv: 1306.3995.
[27] V. S. Shchesnovich, Phys. Rev. A **89**, 022333 (2014).
[28] C. W. J. Beenakker, Rev. Mod. Phys. **69**, 731 (1997).
[29] G. Berkolaiko and J. Kuipers, Phys. Rev. E **85**, 045201 (2012); J. Math. Phys. (N.Y.) **54**, 112103 (2013).
[30] K. Richter and M. Sieber, Phys. Rev. Lett. **89**, 206801 (2002).
[31] S. Müller, S. Heusler, A. Altland, P. Braun, and F. Haake, New J. Phys. **11**, 103025 (2009).
[32] R. K. Badhuri and M. Brack, *Semiclassical Physics* (Addison-Wesley, Reading, MA, 1997).
[33] L. S. Schulman, *Techniques and Applications of Path Integration* (John Wiley & Sons, New York, 1981); M. Gutzwiller, *Chaos in Classical and Quantum Mechanics* (Springer, New York, 1990).
[34] C. W. J. Beenakker, J. W. F. Venderbos, and M. P. van Exter, Phys. Rev. Lett. **102**, 193601 (2009).
[35] M. Candé and S. E. Skipetrov, Phys. Rev. A **87**, 013846 (2013).

[36] M. Candé, A. Goetschy, and S. E. Skipetrov, Europhys. Lett. **107**, 54004 (2014).
[37] A. Arkhipov and G. Kuperberg, Geom. Topol. Monogr. **18**, 1 (2012).
[38] J. J. Sakurai, *Modern Quantum Mechanics* (Addison-Wesley, Reading, MA, 1967).
[39] E. Bocquillon, V. Freulon, F. D. Parmentier, J.-M. Berroir, B. Placais, C. Wahl, J. Rech, T. Jonckheere, T. Martin, C. Grenier, D. Ferraro, P. Degiovanni, and G. Feve, Ann. Phys. (Berlin) **526**, 1 (2014).
[40] C. W. J. Beenakker, C. Emary, M. Kindermann, and J. L. van Velsen, Phys. Rev. Lett. **91**, 147901 (2003).
[41] D. Waltner, *Semiclassical Approach to Mesoscopic Systems* (Springer, Heidelberg, 2012).
[42] See Supplemental Material at http://link.aps.org/supplemental/10.1103/PhysRevLett.116.100401, Sec. III, Eq. 50, for the derivation of Eq. (7).
[43] J. Kuipers and M. Sieber, Phys. Rev. E **77**, 046219 (2008).
[44] See Supplemental Material at http://link.aps.org/supplemental/10.1103/PhysRevLett.116.100401, Sec. 1, Eqs. (1)–(3), for the derivation of Eq. (11).
[45] M. C. Tichy, K. Mayer, A. Buchleitner, and K. Molmer, Phys. Rev. Lett. **113**, 020502 (2014).
[46] V. S. Shchesnovich, arXiv:1403.4459.
[47] See Supplemental Material at http://link.aps.org/supplemental/10.1103/PhysRevLett.116.100401, Sec. II, Eqs. (15), (18), (24), and (27), for the derivation of Eqs. (13) and (14).
[48] T. Engl, J. Dujardin, A. Arguelles, P. Schlagheck, K. Richter, and J. D. Urbina, Phys. Rev. Lett. **112**, 140403 (2014).
[49] See Supplemental Material at http://link.aps.org/supplemental/10.1103/PhysRevLett.116.100401, Sec. IV A, for the semiclassical derivation of Eq. (15).
[50] See Supplemental Material at http://link.aps.org/supplemental/10.1103/PhysRevLett.116.100401, Sec. IV B, for the generalization of Eq. (15) for non-zero mismatch.
[51] See Supplemental Material at http://link.aps.org/supplemental/10.1103/PhysRevLett.116.100401, Sec. IV C, for the derivation of Eq. (16).
[52] See Supplemental Material at http://link.aps.org/supplemental/10.1103/PhysRevLett.116.100401, Sec. III D, Eqs. (68)–(77), for the calculation of this variance, which includes Refs. [53–62].
[53] P. W. Brouwer and C. W. J. Beenakker, J. Math. Phys. (N.Y.) **37**, 4904 (1996).
[54] G. Berkolaiko and J. Kuipers, J. Math. Phys. (N.Y.) **54**, 123505 (2013).
[55] J. Novak, Electron. J. Comb. **14**, R21 (2007).
[56] S. Matsumoto, Random Matrices Theory Appl. **01**, 1250005 (2012).
[57] S. Matsumoto, Random Matrices Theory Appl. **02**, 1350001 (2013).
[58] G. Berkolaiko and J. Kuipers, New J. Phys. **13**, 063020 (2011).
[59] S. Müller, S. Heusler, P. Braun, and F. Haake, New J. Phys. **9**, 12 (2007).
[60] G. Berkolaiko, J. M. Harrison, and M. Novaes, J. Phys. A **41**, 365102 (2008).
[61] N. J. A. Sloane, The On-Line Encyclopedia of Integer Sequences, http://www.research.att.com/njas/sequences/.
[62] S. Aaronson and A. Arkhipov, Theory Comput. **9**, 143 (2013).